Design of a Novel Compliant Safe Robot Joint With Multiple Working States

Zerui Wang, *Student Member, IEEE*, Hiu Man Yip, *Student Member, IEEE*, David Navarro-Alarcon, *Member, IEEE*, Peng Li, Yun-hui Liu, *Fellow, IEEE*, Dong Sun, *Fellow, IEEE*, Hesheng Wang, *Senior Member, IEEE*, and Tak Hong Cheung

***Abstract*—This paper presents the design and development of a novel compliant safe joint (CSJ). The principle of operation of the CSJ is based on a cam-like transmission mechanism, which we call the bridge. The cam profile on the stationary bridge is designed to have multiple regions, which allow the CSJ to passively achieve multiple working states. The proposed joint behaves as a normal rigid joint when the load is smaller than a preset threshold, shifts into the flexible state when the load exceeds the threshold, and switches into the free state in which the motion cannot be transmitted from the motor to the output shaft. In order to achieve a compact modular assembly, the joint's components are designed to have the shape of a hollow cylinder and to be installed around the motor. We analyze how the key dimension parameters affect the torque threshold and the joint's stiffness. Experiments are conducted to validate the working principle and verify the performance of the joint.**

***Index Terms*—Compliant joint, mechanical design, physical human–robot interaction, safety.**

I. Introduction

With the incorporation of robotics into our daily life, many researchers have paid a lot of attention to safety problems arising from physical human–robot interactions [1]–[3], especially in service and surgical applications where safety requirements are much stricter [4]. Note that most actuators available are essentially rigid, therefore, their use in service and surgical robots will inevitably cause safety problems when unwanted interactions or collisions occur [5]–[7]. The installation of compliant joints in surgical robots can improve safety, as these passive devices can absorb part of impact energy when a robot collides with the human body.

In order to introduce compliance into our actuators, we can mainly use two kinds of approaches: the active approach and the passive approach. Compliance in the active approach is produced from an action of a control system, i.e., the control algorithm guarantees that the closed-loop dynamics of the system behaves like a flexible mechanical structure. Thus, an active compliant system has high programmability [8], [9], however, it completely relies on sensors and computer algorithm. Compared to the active approach [10], the passive approach generates compliance from a mechanical design perspective, i.e., by introducing flexible mechanical structures into joint. Passive compliant systems can provide a faster and sensor-less response to unexpected collisions, and its implementation cost is relatively low since there is no need for embedding various sensors and controls.

There are a lot of compliant or flexible joints developed by many researchers. The VSA and VSA-II were developed by Schiavi and Tonietti *et al.* [11], [12]. The VSA has a timing transmission belt tensioned by springs that connects the main shaft to the antagonistic pair of actuators. In the design of VSA-II, the nonlinear torque-displacement relationship can be achieved by a combination of a four-bar mechanism and a linear spring. The AwAS and AwAS-II were developed by Jafari *et al.* [13], [14]. And Tsagarakis *et al.* developed the CompAct-VSA [15]. In the design of these systems, a lever mechanism and antagonistic springs are used to generate compliance. Choi *et al.* developed the VSJ, which has controllable stiffness using a leaf spring with two motors [16]. Park and Chung in [17] developed the FJR, in which a flexible unit, called Flexure Pivot, is connected in series to produce compliance. In [18], Koganezawa *et al.* developed an actuator with a nonlinear elastic system, which can achieve the nonlinear elasticity by using a combination of a torsion spring and a guide-shaft whose diameter gradually changes along the rotation axis. The actuators mentioned above are capable of generating flexibility in a passive way. However, there are some drawbacks such as big volume, a single working state (i.e., these joints only have a flexible working mode) and incapability of automatic state switching.

In this paper, we propose a novel design of the compliant safe joint (CSJ). The joint has passive adjustable compliance: it can work as a common rigid motor when the working load is smaller than a threshold, and shifts into a flexible state when the working load exceeds the threshold. Instead of simply

Manuscript received May 18, 2015; revised July 26, 2015 and October 27, 2015; accepted November 8, 2015. Date of publication November 13, 2015; date of current version February 24, 2016. Recommended by Technical Editor J. Ryu. This work was supported in part by the Hong Kong Research Grants Council under Grant 415011 and under Grant CUHK6/CRF/13G and the Hong Kong Innovation and Technology Fund Under Grant ITS/020/12FP.

Z. Wang, H. M. Yip, D. Navarro-Alarcon, and Y.-H. Liu are with the Department of Mechanical and Automation Engineering, The Chinese University of Hong Kong, HKSAR, Hong Kong (e-mail: zrwang@mae.cuhk.edu.hk; hmyip@mae.cuhk.edu.hk; dnavarro@mae.cuhk.edu.hk; yhliu@mae.cuhk.edu.hk).

P. Li is with the Department of Mechanical and Automation Engineering, The Chinese University of Hong Kong, HKSAR, Hong Kong, and also with the School of Mechanical Engineering and Automation, Harbin Institute of Technology, Shenzhen Graduate School, Shenzhen 518055, China (e-mail: pli@mae.cuhk.edu.hk; lipeng@hitsz.edu.cn).

D. Sun is with the Department of Mechanical and Biomedical Engineering, City University of Hong Kong, HKSAR, Hong Kong (e-mail: medsun@cityu.edu.hk).

H. Wang is with the Department of Automation, School of Electronic, Information, and Electrical Engineering, Shanghai Jiao Tong University, Shanghai 200240, China (e-mail: wanghesheng@sjtu.edu.cn).

T. H. Cheung is with the Department of Obstetrics and Gynaecology, Prince of Wales Hospital, HKSAR, Hong Kong (e-mail: thcheung@cuhk.edu.hk).

Color versions of one or more of the figures in this paper are available online at http://ieeexplore.ieee.org.

Digital Object Identifier 10.1109/TMECH.2015.2500602

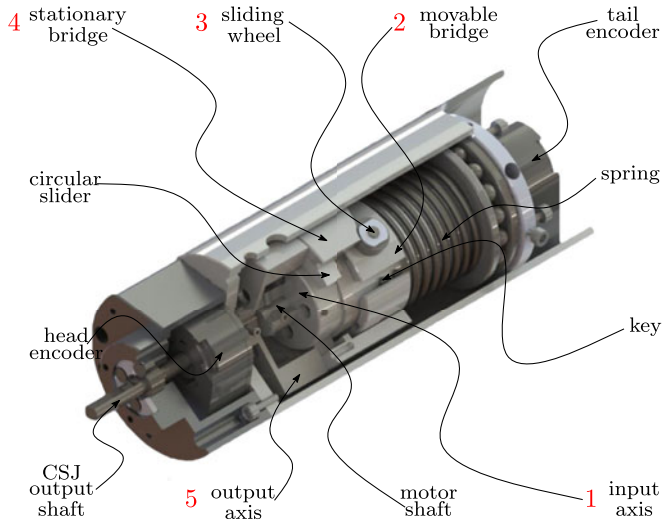

Fig. 1. Part sectioned view of the CSJ's assembly showing the torque transmission chain.

connecting a flexible unit to the front of the motor (e.g., in [17]), part of the components are designed to have the shape of a hollow cylinder so that they can be placed around the motor. This kind of design results in a compact mechanical structure (the joint has 60 mm diameter and 180 mm length). We report experiments with robotic prototypes evaluate the performance of the proposed device. Preliminary design concepts and simple control methods of the CSJ were presented in [19]. We extend our previous study by analyzing how the key dimension parameters affect the joint's performance with experimental studies of the joint itself and the integration with a surgical robot prototype.

The rest of this manuscript has the following structure: In Section II, we present the design of the joint. In Section III, we present the conducted experiments. Limitations and future improvements are discussed in Section IV.

II. Design of the CSJ

In this section, we detail the design of the proposed CSJ.

A. Design Requirements

The design is based on the following requirements: First, the CSJ should exhibit passive and adjustable stiffness. Second, it should have multiple working states. Finally, it should be compact. Passive compliance can be achieved by incorporating a flexible unit (e.g., a spring) into the joint and the stiffness can be adjusted by changing the effective length or initial load of the spring. By introducing a cam-like transmission mechanism (here called the bridge) whose cam profile has multiple regions such that the joint can achieve multiple working states. This bridge converts the linear compliance of the spring into a rotational one. Instead of connecting the high-gear-ratio dc motor in series with the compliant unit, we place the components surrounding the motor so that the mechanical structure is much more compact. The part sectioned view of the CSJ is shown in Fig. 1. The working principle of the CSJ is shown in Fig. 2.

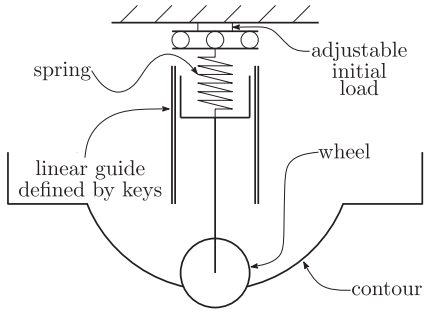

Fig. 2. Schematics of the joint's working principle.

B. Torque Transmission Chain

As shown in Fig. 1, the output torque of the motor is transmitted from the motor shaft to the CSJ's output shaft through the following torque transmission chain: 1 *input axis* → 2 *movable bridge* → 3 *wheels* → 4 *stationary bridge* → 5 *output axis*.

The *input axis* connected to the dc-motor's shaft has several keys for providing a guide on which the movable bridge can slide along. The *movable bridge*, which is circumferentially mounted on the input axis, has an inner surface on which four slide rails are provided for receiving the pins, such that the movable bridge slides along the axial direction of the input axis. Two *wheels* connect the movable and stationary bridge. Each of the wheels has an inner ring and an outer ring. The inner ring is fixed to the movable bridge and the outer ring stays in the slot or moves along the helicoid surface of the stationary bridge. The *stationary bridge*, mounted on the input axis by a circular slider, can only rotate with respect to the input axis.

The concept of "movable" or "stationary" is defined according to the relative motion of the bridges with respect to the input axis. The movable bridge can only move along the axial direction of the input axis and the stationary bridge can only rotate around the input axis.

The compliance of the CSJ is generated by a linear *spring*. We introduce a special transmission mechanism, i.e., the bridge, to convert linear compliance into rotational compliance. When the working load is below the preset threshold, the bridges (both stationary and movable) are static with respect to the motor shaft, and the output torque τ_{CSJ} equals to the output torque τ_m of the motor. When the working load is large and exceeds the threshold, the wheels go out of the stationary bridge's slots. The stationary and movable bridges have relative rotational and linear motion that compresses the spring with respect to the motor shaft, respectively. Under this situation, the output torque τ_{CSJ} of the CSJ roughly equals to the internal torque τ_i produced by the spring, which is much smaller than the maximum output torque $\tau_{\text{CSJ}_{\max}}$ of the CSJ.

C. Rigid, Flexible, and Free State

One of the innovative features of the CSJ is that it has multiple working states, which results from the cam profile of the stationary bridge. There are totally six regions in our device, see Fig. 3. The region 1 represents the rigid state; the region $1 \leftrightarrow 2$,[1]

[1]We use $\leftrightarrow$ to represent the interval of a region.

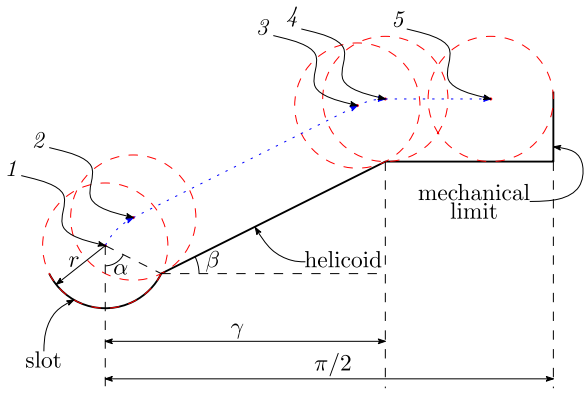

Fig. 3. Schematics of the dimensions of the stationary bridge and the characteristic positions of the wheels moving along the surface of the stationary bridge. Only one quarter of the hollow cylinder is sketched in an unfolding view. Black solid arc and lines represent the slot and the helicoid surface of the stationary bridge, respectively. Red dashed circles and points represent the wheels and their center points, respectively. Blue dotted arc and lines represent the trajectory of the wheel's center.

TABLE I
RIGID, FLEXIBLE, AND FREE REGIONS

Regions	Intervals
Rigid:	$\Delta q = 0$
Rigid $\leftrightarrow$ Flexible:	$\Delta q \in \left(0, \frac{2r}{D}(\sin\alpha - \sin\beta)\right)$
Flexible:	$\Delta q \in \left(\frac{2r}{D}(\sin\alpha - \sin\beta), \gamma - \frac{2r}{D}\sin\beta\right)$
Flexible $\leftrightarrow$ Free:	$\Delta q \in \left(\gamma - \frac{2r}{D}\sin\beta, \gamma\right)$
Free:	$\Delta q \in \left(\gamma, \frac{\pi}{2} - \frac{2r}{D}\right)$
Mechanical limit:	$\Delta q = \frac{\pi}{2} - \frac{2r}{D}$

$2 \leftrightarrow 3$, and $3 \leftrightarrow 4$ represent the flexible state; the region $4 \leftrightarrow 5$ is free state, and the region 5 is the mechanical limit.

The CSJ behaves as a rigid joint when the wheels are sitting inside the slots (region 1). The CSJ exhibits compliance when the wheels are out of the slots (region $1 \leftrightarrow 2, 2 \leftrightarrow 3$, and $3 \leftrightarrow 4$). The CSJ cannot transmit torque to the output shaft when the wheels are in the region $4 \leftrightarrow 5$. This case should be avoided, because the mechanical limit can be reached. In that case, there will be a big impulse of interaction force which is dangerous. (The regions can be found in Table I)

By designing the cam profile of the stationary bridge having these multiple regions, as shown in Fig. 3, we can fulfill the second requirement mentioned in the Section II-A. The dimensions of the stationary bridge affect some characteristics such as the effective range of the flexible states, the adjustable interval of the preset threshold, and the compliance under the flexible states. The parameter γ determines the effective range of flexible states. Selection of other dimensions like α and β will be discussed in the following sections. See Fig. 3 for a conceptual representation.

D. Preset Threshold

When the working load exceeds the preset threshold, the CSJ will shift from the rigid state into the flexible state; selecting an appropriate threshold is a crucial issue in the joint design. The value of torque threshold is a function of the geometric dimensions of the stationary bridge, the stiffness, and the initial load of the spring. We can model the torque threshold under a static situation as follows (see Fig. 3)

$$T_r = k(x_0 + x_i)D\tan(\alpha). \tag{1}$$

Table II defines parameters and details are shown in Appendix A.

Our purpose here is to calculate the contact region α given desired threshold value according to (1). Visualization of the relationship is shown in Fig. 4. The sequence of determining the contact region α can be summarized as follows:

1) Draw a horizontal line according to the desired threshold, e.g., 3 Nm, intersecting with minimum and maximum curves at point *B* and *D*, respectively.
2) Draw a vertical line intersecting with minimum ($x_i = 0$ mm) and maximum ($x_i = 20$ mm) curves at point *C* and *A*, respectively. The parameter α can be obtained by letting $\|OA\| = \|OC\|$, so that the desired threshold sits at the optimal midpoint of adjustable interval.

By following the steps above, we can only get an estimation of the desired threshold instead of the practical one. So putting the desired threshold at the midpoint of the adjustable interval gives us enough flexibility to compensate the modeling error.

TABLE II
MODEL PARAMETERS

Symbol	Value	Meaning
T_r	dep. var.	Torque threshold
k	2000 N/m	Stiffness of spring
x_0	10 mm	Initial load of spring
x_i	$[0, 20]$ mm	Adjustable initial load of spring
D	48 mm	Diameter of stationary bridge
α	indep. var.	Contact region between wheels and slots

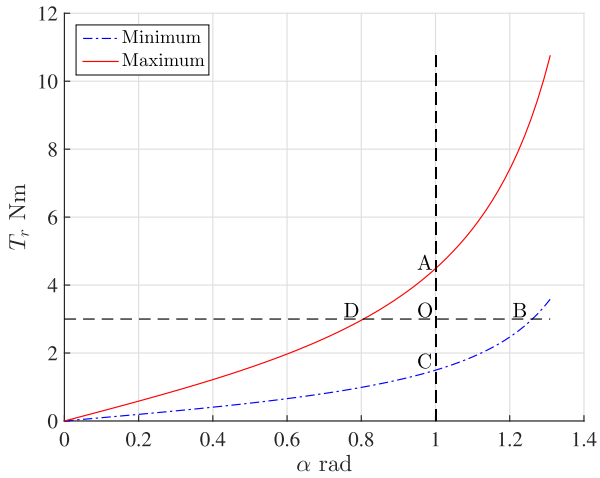

Fig. 4. Preset torque threshold profiles obtained by adjusting initial load of the spring.

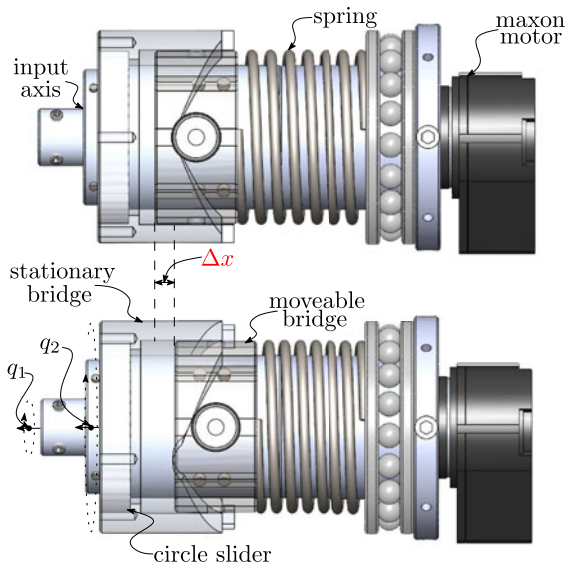

Fig. 5. CAD models of the CSJ showing that the CSJ works under the rigid state (top) and works under the flexible state (bottom).

E. Compliance Under Flexible State

The parameter β determines the compliance of the CSJ when it is working under flexible state. To model the output torque of CSJ, we assume that the joint rotates at slow speed (which often holds in surgical applications). The torque of the joint is as follows:

$$T_f = k(x_0 + x_i + \Delta x)D\tan(\beta) \tag{2}$$

where the distance Δx satisfies

$$\Delta x = \left(\frac{D}{2}\Delta q - (r\sin(\alpha) - r\sin(\beta))\right) + (r\cos(\beta) - r\cos(\alpha)) \tag{3}$$

for $\Delta q = q_2 - q_1$ as an angular displacement error. See Fig. 5.

By substituting (3) into (2), we can get the linear relationship between T_f and Δq as

$$T_f = a\Delta q + b \tag{4}$$

where,

$$a = \frac{kD^2}{2}\tan(\beta) \tag{5}$$

$$b = [r(\cos(\beta) + \sin(\beta) - \cos(\alpha) - \sin(\alpha)) + (x_0 + x_i)]\, kD\tan(\beta). \tag{6}$$

From (5) and (6), we notice that both slope a and intercept b increase at rate of tangent with respect to β. Selection of β should observe the following criterion:

1) Torque at critical position from rigid state to flexible state is smaller than T_r

$$T_f|_{\Delta q = \frac{2r}{D}(\sin(\alpha) - \sin(\beta))} < T_r. \tag{7}$$

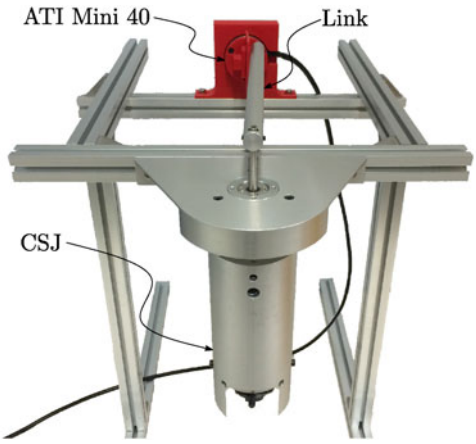

Fig. 6. Fabricated prototype of the CSJ used for the collision experiments. An ATI force transducer was used to measure the contact force.

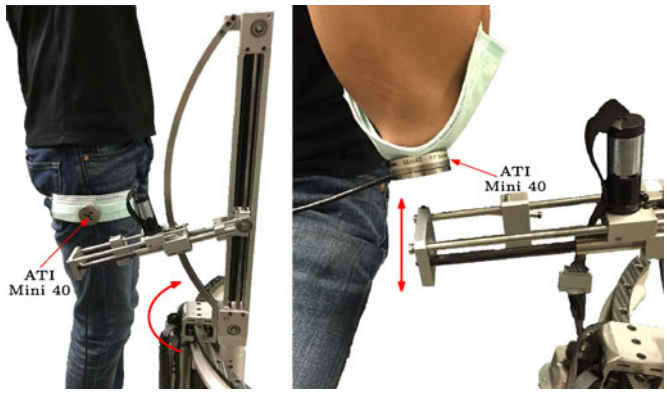

Fig. 7. Experiment setup used for the human–robot collision experiment.

2) Torque at critical position from flexible state to free state is smaller than some known safety value T_s

$$T_f|_{\Delta q = \gamma - \frac{2r}{D}\sin(\beta)} < T_s. \tag{8}$$

III. Experiments

In this section, we present several experiments to evaluate the performance of the CSJ.

A. Setup

The experimental platform for initial load varying experiment consists of a one-DOF robot manipulator, a CSJ, and an ATI Mini 40 force transducer (see Fig. 6). The experimental system for the collision experiment is a surgical robot prototype (see [20] and Fig. 7). The first two joints are actuated by the CSJs. We control the velocities of these CSJs using a Linux-based PC with a Galil DMC-4040 Digital Motion Controller.

B. Initial Load Varying Experiment

The link actuated by the CSJ moved at a constant speed. The link collided with a plate instrumented with the force transducer.

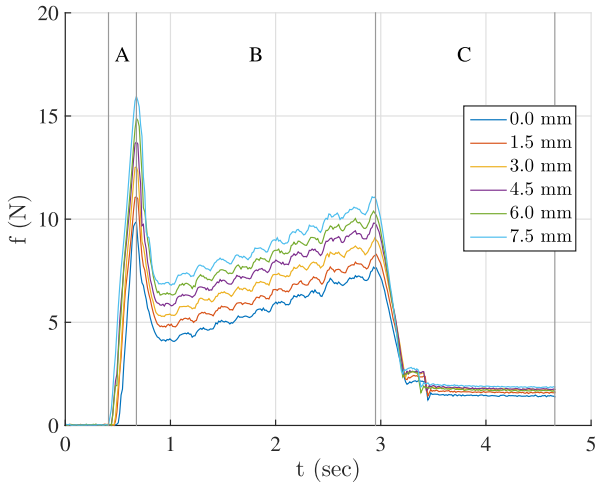

Fig. 8. Force profiles obtained during the initial load varying experiment. The change of the interaction force has three stages: A (rigid state); B (flexible state); and C (free state).

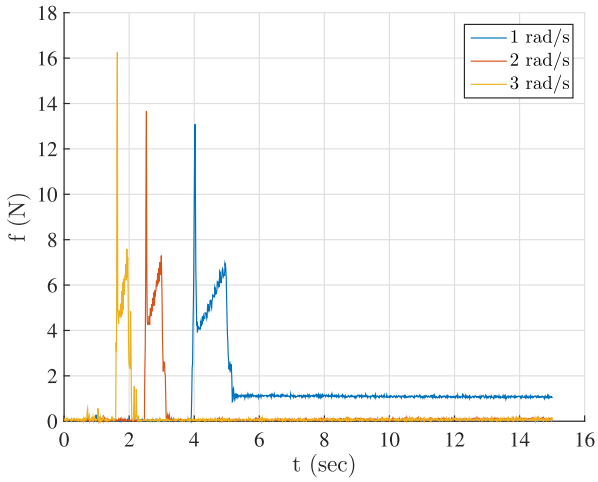

Fig. 9. Force profiles obtained during the impact velocity varying experiment.

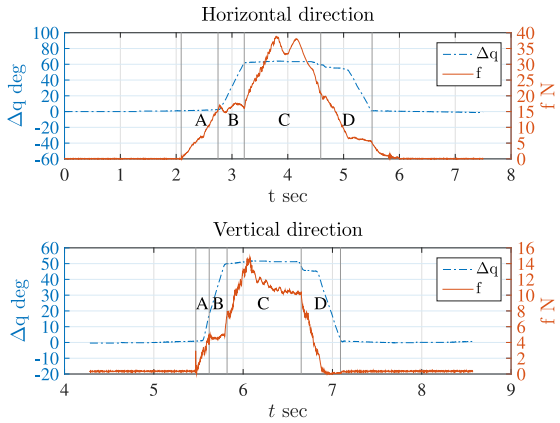

Fig. 10. Force profiles obtained during the human–robot collision experiment.

We conducted this experiment several times with different initial loads of the spring. The initial load was manually adjusted with the screws that compress the spring; we incrementally adjusted them in steps of 1.5 mm. The experimental result is shown in Fig. 8. The collision force represents the magnitude of resultant force acting at the force transducer. According to the measurements of the experiment, we observe that the threshold can be adjusted in a range from 10 to 16 N.

When the working load exceeded the threshold, the output torque dropped to a lower safe value and the CSJ shifted into flexible state, in which the output torque was proportional to the angular position difference between motor and joint. When the CSJ shifted from the flexible state into the free state, the output torque dropped to zero since the mechanical structure at that state could not transmit any torque from the motor to the output axis. The residual torque shown in the experimental result was caused by friction inside the CSJ's mechanical structure.

C. Impact Velocity Varying Experiment

In this experiment, the link actuated by the CSJ moved with a fixed initial spring load. The link collided with a plate instrumented with the force transducer. We conducted this experiment several times with different impact velocities. The experimental result is shown in Fig. 9. We kept the same angular displacement from the link's initial position to the plate for each time. Therefore, the impact with higher velocity took place earlier than those with lower velocities.

According to the results, we notice that the impact pulse with higher impact velocity is larger than those with lower velocities. The duration of flexible state with higher velocity is shorter than those with lower velocities, and the slop of force profile under flexible state is higher than those with lower velocities. All the previous results are the effects of the inertia of the link and joint. When the CSJ is triggered, the impact force will drop into a lower safe value since the CSJ shifts under flexible state.

The residual force caused by the friction only appears in the case of lower velocity (blue line) because big vibrations caused by higher velocities let the link go back a little bit and there is no physical contact between the plate and the link.

D. Collision Experiment

We also tested the performance of the joint when colliding with a human. During these collisions, the interaction force was measured by the force sensor in real time, see Fig. 7. The experimental results are shown in Fig. 10, in which the blue line represents the angular position difference between the motor and the joint and the red solid line represents the interaction force between the human and the robot measured by the force sensor.

According to the experimental results, the change of the interaction force has four stages:

1) A: The interaction force increases, because the CSJs are working under rigid state (i.e., $\Delta q = 0$) and the robot collides with the human.
2) B: The interaction force stops increasing and is fixed at a certain value, because the CSJs shift into the flexible state (i.e., $\Delta q > 0$). Since the friction between the circular slider

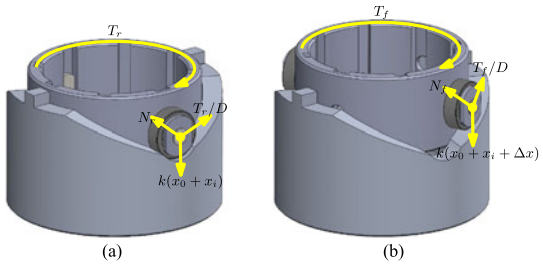

Fig. 11. Free body diagrams of the bridge, which is operating under both rigid and flexible states.

and the stationary bridge is too big, the force remains a constant small value.

3) C: The interaction force increases again, because the CSJs reach the mechanical limit. In the experiment, the spring is fully compressed, which limits the travel of the movable bridge. Hence, the CSJs directly reach mechanical limit instead of shifting into the free state and then reaching the mechanical limit.
4) D: The interaction force decreases to zero, because the robot is commanded to move backward. Finally, the CSJs shift back to the rigid state (i.e., $\Delta q = 0$).

Although the period of the stage B is short, the Δq is big enough to be an indicator for stopping the robot immediately. For example, in the hysterectomy assisted by the surgical robot assistant mentioned in the Section III-A, we implement the algorithm to stop the robot when the Δq is greater than a certain value such that the robot will be automatically disabled when it collides with the patient's body.

IV. Conclusion

In this paper, we first introduce a novel design of CSJ. The joint is designed for high gear ratio dc motors and has passive adjustable compliance. The mechanical structure of the CSJ is compact, i.e., the joint diameter is 60 mm and the joint length is 180 mm. The CSJ has multiple working states so that it can work as common rigid motor when the working load is smaller than a threshold and shifts into flexible state when the working load exceeds the threshold. Finally, we validated the proposed device and verified the performance by experiments.

In contrast with other compliant or flexible joints, the CSJ introduced in this paper has multiple working states so that the compliance only appears when needed, i.e., working load exceeds a predetermined threshold. Moreover, its compact size allows it to be easily installed on robotic systems.

In the future, we plan to modularize the CSJ and develop a multidegree-freedom robot with the CSJ installed on each of its joint. We would also like to develop a motion control algorithm for this new mechatronic device.

Appendix A

According the free body diagram shown in Fig. 11(a), we can obtain

$$\frac{T_r}{D} = k(x_0 + x_i)\tan(\alpha).$$

Similarly, we can obtain the equation for flexible state

$$\frac{T_f}{D} = k(x_0 + x_i + \Delta x)\tan(\beta).$$

The angles in the tangent functions above are different because of the different slopes under rigid and flexible states.

References

[1] Y. Yamada, Y. Hirasawa, S. Huang, Y. Umetani, and K. Suita, "Human-robot contact in the safeguarding space," *IEEE/ASME Trans. Mechatronics*, vol. 2, no. 4, pp. 230–236, Dec. 1997.
[2] A. Bicchi, M. A. Peshkin, and J. E. Colgate, "Safety for physical human–robot interaction," in *Springer Handbook of Robotics*. New York, NY, USA: Springer, 2008, pp. 1335–1348.
[3] A. Bicchi, M. Bavaro, G. Boccadamo, D. De Carli, R. Filippini, G. Grioli, M. Piccigallo, A. Rosi, R. Schiavi, S. Sen, and G. Tonietti,, "Physical human-robot interaction: Dependability, safety, and performance," in *Proc. 10th IEEE Int. Workshop Adv. Motion Control*, 2008, pp. 9–14.
[4] R. H. Taylor and D. Stoianovici, "Medical robotics in computer-integrated surgery," *IEEE Trans. Robot. Autom.*, vol. 19, no. 5, pp. 765–781, Oct. 2003.
[5] N. Hogan, "Impedance control: An approach to manipulation: Part ii—implementation," *J. Dynamic Syst., Meas., Control*, vol. 107, no. 1, pp. 8–16, 1985.
[6] D. B. Camarillo, T. M. Krummel, and J. K. Salisbury, "Robotic technology in surgery: Past, present, and future," *Amer. J. Surg.*, vol. 188, no. 4, pp. 2–15, 2004.
[7] A. De Luca, A. Albu-Schaffer, S. Haddadin, and G. Hirzinger, "Collision detection and safe reaction with the dlr-iii lightweight manipulator arm," in *Proc. IEEE/RSJ Int. Conf. Intell. Robots Syst.*, 2006, pp. 1623–1630.
[8] C. A. Klein and R. L. Briggs, "Use of active compliance in the control of legged vehicles," *IEEE Trans. Syst., Man Cybern.*, vol. 10, no. 7, pp. 393–400, Jul. 1980.
[9] B. R. Shetty and V. Ang, "Active compliance control of a puma 560 robot," in *Proc. IEEE Int. Conf. Robot. Autom.*, 1996, vol. 4, pp. 3720–3725.
[10] W. Wang, R. N. Loh, and E. Y. Gu, "Passive compliance versus active compliance in robot-based automated assembly systems," *Ind. Robot: Int. J.*, vol. 25, no. 1, pp. 48–57, 1998.
[11] G. Tonietti, R. Schiavi, and A. Bicchi, "Design and control of a variable stiffness actuator for safe and fast physical human/robot interaction," in *Proc. IEEE Int. Conf. Robot. Autom.*, 2005, pp. 526–531.
[12] R. Schiavi, G. Grioli, S. Sen, and A. Bicchi, "Vsa-ii: A novel prototype of variable stiffness actuator for safe and performing robots interacting with humans," in *Proc. IEEE Int. Conf. Robot. Autom.*, 2008, pp. 2171–2176.
[13] A. Jafari, N. G. Tsagarakis, B. Vanderborght, and D. G. Caldwell, "A novel actuator with adjustable stiffness (awas)," in *Proc. IEEE/RSJ Int. Conf. Intell. Robots Syst.*, 2010, pp. 4201–4206.
[14] A. Jafari, N. G. Tsagarakis, and D. G. Caldwell, "Awas-ii: A new actuator with adjustable stiffness based on the novel principle of adaptable pivot point and variable lever ratio," in *Proc. IEEE Int. Conf. Robot. Autom.*, 2011, pp. 4638–4643.
[15] N. G. Tsagarakis, I. Sardellitti, and D. G. Caldwell, "A new variable stiffness actuator (compact-vsa): Design and modelling," in *Proc. IEEE/RSJ Int. Conf. Intell. Robots Syst.*, 2011, pp. 378–383.
[16] J. Choi, S. Hong, W. Lee, S. Kang, and M. Kim, "A robot joint with variable stiffness using leaf springs," *IEEE Trans. Robot.*, vol. 27, no. 2, pp. 229–238, Apr. 2011.
[17] Y. J. Park and W. K. Chung, "External torque sensing algorithm for flexible-joint robot based on disturbance observer structure," in *Proc. IEEE/RSJ Int. Conf. Intell. Robots Syst.*, 2014, pp. 4735–4741.
[18] K. Koganezawa, H. Inomata, and T. Nakazawa, "Actuator with non-linear elastic system and its application to 3 dof wrist joint," in *Proc. IEEE Int. Conf. Mechatronics Autom.*, 2005, vol. 3, pp. 1253–1260.
[19] Z. Wang, P. Li, D. Navarro-Alarcon, H. M. Yip, Y.-H. Liu, W. Lin, and L. Li, "Design and control of a novel multi-state compliant safe joint for robotic surgery," in *Proc. IEEE Int. Conf. Robot. Autom.*, 2015, pp. 1023–1028.
[20] H. M. Yip, Z. Wang, D. Navarro-Alarcon, P. Li, and Y. Liu, "A new robotic uterine positioner for laparoscopic hysterectomy with passive safety mechanisms: Design and experiments," in *Proc. IEEE Int. Conf. Intell. Robots Syst.*, 2015, pp. 3188–3194.